

Steps towards a ^{229}Th ionic nuclear clock in a linear ion trap

Wen-Ting Gan(甘文婷), Zi Li(李梓), Chen Wang(王晨), Xia Hua(华夏), and Xin Tong(童昕)
Citation: Chin. Phys. B, 2026, 35 (**2**): 023703. DOI: 10.1088/1674-1056/ae31db
http://cpb.iphy.ac.cn; http://iopscience.iop.org/cpb

What follows is a list of articles you may be interested in

Research on the ions' axial temperature of a sympathetically-cooled $^{113}Cd^{+}$ ion crystal

Nong-Chao Xin(辛弄潮), Sheng-Nan Miao(苗胜楠), Hao-Ran Qin(秦浩然), Li-Ming Guo(郭黎明), Ji-Ze Han(韩济泽), Hua-Xing Hu(胡华星), Wen-Xin Shi(施文心), Jian-Wei Zhang(张建伟), and Li-Jun Wang(王力军)
Chin. Phys. B, 2021, 30 (**11**): 113701. DOI: 10.1088/1674-1056/abe379

Numerical analysis of motional mode coupling of sympathetically cooled two-ion crystals

Li-Jun Du(杜丽军), Yan-Song Meng(蒙艳松), Yu-Ling He(贺玉玲), and Jun Xie(谢军)
Chin. Phys. B, 2021, 30 (**7**): 073702. DOI: 10.1088/1674-1056/abfc3e

Ground state cooling of an optomechanical resonator with double quantum interference processes

Shuo Zhang(张硕), Tan Li(李坦), Qian-Hen Duan(段乾恒), Jian-Qi Zhang(张建奇), and Wan-Su Bao(鲍皖苏)
Chin. Phys. B, 2021, 30 (**2**): 023701. DOI: 10.1088/1674-1056/abc2c0

Quantitative evaluation of space charge effects of laser-cooled three-dimensional ion system on a secular motion period scale

Li-Jun Du(杜丽军), Hong-Fang Song(宋红芳), Shao-Long Chen(陈邵龙), Yao Huang(黄垚), Xin Tong(童昕), Hua Guan(管桦), Ke-Lin Gao(高克林)
Chin. Phys. B, 2018, 27 (**4**): 043701. DOI: 10.1088/1674-1056/27/4/043701

Compensating for excess micromotion of ion crystals

Du Li-Jun (杜丽军), Chen Ting (陈婷), Song Hong-Fang (宋红芳), Chen Shao-Long (陈邵龙), Li Hai-Xia (李海霞), Huang Yao (黄垚), Tong Xin (童昕), Guan Hua (管桦), Gao Ke-Lin (高克林)
Chin. Phys. B, 2015, 24 (**8**): 083702. DOI: 10.1088/1674-1056/24/8/083702

TOPICAL REVIEW — Advances in thorium nuclear optical clocks

Steps towards a ^{229}Th ionic nuclear clock in a linear ion trap

Wen-Ting Gan(甘文婷)[1,2], Zi Li(李梓)[1,2], Chen Wang(王晨)[1,2], Xia Hua(华夏)[1,†], and Xin Tong(童昕)[1,3,‡]

[1] *Innovation Academy for Precision Measurement Science and Technology, Chinese Academy of Sciences, Wuhan* 430071, *China*
[2] *University of Chinese Academy of Sciences, Beijing* 100049, *China*
[3] *Wuhan Institute of Quantum Technology, Wuhan* 430206, *China*

(Received 30 August 2025; revised manuscript received 12 November 2025; accepted manuscript online 30 December 2025)

Owing to the presence of a low-energy, long-lived nuclear isomeric state, ^{229}Th is an ideal candidate for developing the next generation clock — the nuclear clock — holding great promise for both applied and fundamental physics. The ^{229}Th ionic nuclear optical clock has garnered considerable attention, attributed to its high precision with a relative uncertainty of $\leq 1.5 \times 10^{-19}$ and the potential for common-mode noise cancellation via self-comparison between the nuclear transition and the electronic transition of thorium ions. In this article, we focus on Th^{n+} ions ($n = 1, 2, 3$) and present a comprehensive review of the current progress in the development of ionic nuclear clocks, covering essential steps such as ion generation, trapping, and cooling. Furthermore, we discuss the realization of a closed-loop clock cycle, addressing key aspects including stable isomer excitation and efficient isomer deexcitation.

Keywords: ^{229}Th ionic nuclear clock, ion generation, ion trapping and cooling, closed-loop clock cycle

PACS: 37.10.Rs, 37.10.Ty, 95.55.Sh

DOI: 10.1088/1674-1056/ae31db **CSTR:** 32038.14.CPB.ae31db

1. Introduction

Today's most precise time and frequency measurements are performed with optical atomic clocks, which play a pivotal role in various fields, such as the global navigation satellite systems,[1–3] the synchronous communication networks,[4] the time reference,[5,6] and the fundamental physics research.[7–9] However, a new type of clock, called a "nuclear clock", is under development. It employs a nuclear transition instead of an atomic shell transition for precise time measurement.[10,11] With a first nuclear excitation state of only ~ 8.4 eV and a radiative lifetime of $\sim 10^3$ s,[12] ^{229}Th is the sole candidate for developing a nuclear clock among currently known nuclides.

A nuclear clock based on the nuclear transition of ^{229}Th is theoretically capable of achieving a systematic uncertainty of 1.5×10^{-19},[11] outperforming state-of-the-art atomic clocks, as shown in Table 1. First, the exceptionally low blackbody radiation (BBR) shift uncertainty in the ^{229}Th nuclear clock arises from its nuclear transition between nuclear states with identical electronic configurations. This symmetry results in a differential polarizability $\Delta\alpha_s$ of $\sim 10^{-5} a_0^3$,[11] which is 7–8 orders of magnitude smaller than those of electronic transitions in ^{87}Sr,[13] $^{27}Al^+$,[14] or $^{40}Ca^+$[15] clocks. Therefore, the clock uncertainty from the BBR shift is 1.3×10^{-22} at room temperature,[11] surpassing the limits of present atomic clocks. Second, owing to the atomic nucleus being about five orders of magnitude smaller than the electron shell, its magnetic dipole moment is significantly smaller than that of electrons, making nuclear clocks less susceptible to magnetic field than atomic clocks. Consequently, the systematic uncertainties arising from the Zeeman effect are reduced by an order of magnitude compared to atomic clocks. Third, the Stark effect contributes minimally to the overall uncertainty of the nuclear clock, which is exceptionally low. This remarkable insensitivity originates from the extremely small differential nuclear polarizability ($\Delta\alpha^{\mathrm{nuc}} < 10^{-14} a_0^3$)[11] and the highly effective shielding of the nucleus from external electric fields by the surrounding electron cloud. For all these reasons, this new type of clock is being considered for applications such as searching for the temporal variations in the fine-structure constant,[16,17] detecting the dark matter,[18,19] serving as a gravitational wave detector,[7] and applying to the chronometric geodesy.[20]

To develop a nuclear clock, the first step is to precisely measure the transition frequency from the ground state to the isomeric state. Since Kroger and Reich observed the existence of an extremely low-lying first excited state of ^{229}Th nuclei in 1976,[21] extensive investigations into the energy of this isomeric state have been carried out via γ-ray spectroscopy,[22–28] internal conversion (IC) electron spectroscopy,[29] and direct vacuum ultraviolet (VUV) spectroscopy,[30,31] as shown in Fig. 1(a). With the successful preparation of ^{229}Th-doped crystals and the development of VUV lasers, significant progress has been made in energy measurement as illustrated in Fig. 1(b). In 2024, a ^{229}Th-doped CaF_2 crystal grown

†Corresponding author. E-mail: huaxia@apm.ac.cn
‡Corresponding author. E-mail: tongxin@apm.ac.cn

© 2026 Chinese Physical Society and IOP Publishing Ltd. All rights, including for text and data mining, AI training, and similar technologies, are reserved.

at the Technische Universität Wien[32] was irradiated with a nanosecond-pulsed VUV laser generated at the Physikalisch-Technische Bundesanstalt (PTB) and the first resonant excitation was observed.[33] This result was soon independently verified using a ^{229}Th-doped $LiSrAlF_6$ crystal at the University of California-Los Angeles (UCLA).[34] Building on these experiments, researchers at the Joint Institute for Laboratory Astrophysics (JILA) used a VUV frequency comb to directly excite the narrow ^{229}Th nuclear clock transition in a ^{229}Th:CaF_2 crystal, improving the measurement result to the kHz level.[35] Soon afterwards, JILA also first achieved nuclear excitation in $^{229}ThF_4$ thin films on MgF_2 and Al_2O_3 substrates, respectively.[36] Lately, Elwell *et al.* obtained the first laser-based conversion electron Mössbauer spectroscopy of ^{229}Th in a thin sample of $^{229}ThO_2$.[37] While the above measurements were conducted on Th^{4+} ions, theoretical calculations revealed a −639 MHz clock transition frequency shift between Th^{3+} and Th^{4+} ions due to electron-induced nuclear frequency shifts.[38]

Table 1. Comparison of systematic uncertainties among the 1D ^{87}Sr optical lattice clock, $^{27}Al^+$ quantum logic clock, liquid-nitrogen-cooled $^{40}Ca^+$ ion optical clock, and $^{229}Th^{3+}$ nuclear clock. All values correspond to fractional frequency uncertainties.

Uncertainty (10^{-19})	^{87}Sr[13]	$^{27}Al^+$[14]	$^{40}Ca^+$[15]	$^{229}Th^{3+}$[11]
Blackbody radiation	7.3	1.7	3.5	0.0013
Second order Zeeman	1.0	2.5	1.4	0
First order Zeeman	0.7		0.2	0.1
Laser Stark	3.2	2.4	0.6	0.5
Background collisions	0.5	0.4	1.8	0.1
Excess micromotion		1.6	1.4	1
Secular motion		3.8	0.4	0.1
Density	0.9			
AOM phase chirp		< 1	1.0	
Gravitational				1
Other effects	0.1	< 1	0.1	0.3
Total	8.2	5.5	4.7	1.5

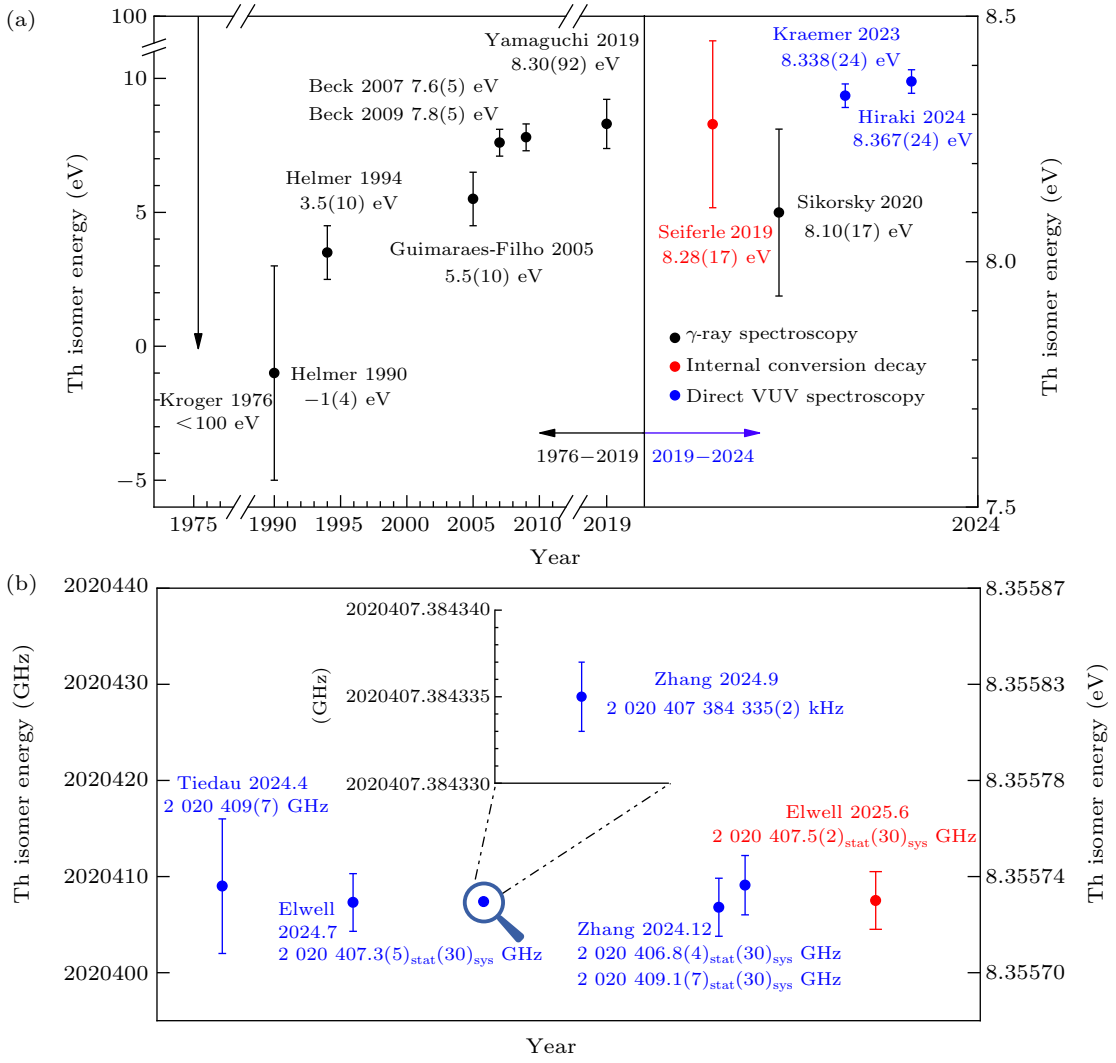


Fig. 1. Development of ^{229}Th nuclear transition measurements. (a) Energy measurements over the past half century. The black, red, and blue points represent the results based on γ-ray spectroscopy, internal conversion decay, and direct VUV spectroscopy, respectively. The left panel represents Th isomer energy measurements from 1976 to 2019 with low precision and the right panel is an enlarged view showing four results from 2019 to 2024 at the THz level. (b) Recent six high-precision results below the THz level. To date, the most precise measurement of the nuclear transition frequency is from Zhang *et al.*, with the precision improved by approximately six orders of magnitude to the kHz level.

With the determination of nuclear transition frequency, various ^{229m}Th-based nuclear clock concepts are discussed. Two primary ones are the ionic nuclear clock and the solid-state nuclear clock.[10,39] The ionic nuclear clock scheme is based on a single $^{229}Th^{3+}$ ion or a Coulomb crystal of $^{229}Th^{3+}$ ions. These ions can be stably trapped for extended periods in an ion trap, effectively isolating them from environmental perturbations and creating favorable conditions for time measurement. For the solid-state nuclear clock scheme, the approach utilizes VUV-transparent crystals doped with ^{229}Th, aiming to directly excite the nuclear clock transition using a VUV laser. The solid-state path requires parallel advancements in generating a narrow-linewidth, high-intensity VUV laser for excitation, and in developing high-purity-doped crystals to amplify the signal for achieving a measurable signal-to-noise ratio.

Detailed performance metrics of the ionic and solid-state nuclear clocks are summarized in Table 2. Among various nuclear clock concepts, the solid-state nuclear clock concept offers compelling advantages for practical applications. The internal conversion electron Mössbauer spectroscopy (CEMS) scheme in ThO_2 enables an exceptionally short interrogation cycle due to its ~ 10 μs isomer lifetime, theoretically boosting short-term stability by eight orders of magnitude compared to radiative approaches, leading to a projected clock instability of $\sim 2\times10^{-18}$ at 1 s.[37] The large ensemble of nuclei (10^{15}–10^{18} cm^{-3} [32,34,40]) provides a signal enhancement over ionic systems. The maturity of the thin-film deposition techniques, as demonstrated with ThF_4, facilitates the development of low-radioactivity, integrated devices, paving the way for portable, chip-scale nuclear clocks.[41] While the solid-state nuclear clocks offer superior short-term stability and integration potential, they still face greater challenges. For thorium-doped crystals, the nuclear transition in the solid-state environment is influenced by electronic charge density, electric field gradient, and field gradient asymmetry at the nucleus, all of which are temperature-dependent. To reach a precision of 10^{-18}, a stable crystal temperature of 5 μK is required.[41] The internal-conversion-based ThO_2 nuclear clock is even more limited, with its precision constrained to $\sim 7.9\times10^{-12}$ due to the isomer lifetime broadening of $2\pi\times16$ kHz.[37] By contrast, the single-ion nuclear clock demonstrates a clear advantage in systematic uncertainty, with a fractional inaccuracy projected to reach 1.5×10^{-19}.[11] Additionally, comparing the nuclear transition and the electronic transition of thorium ion system offers an opportunity to measure temporal variations in the fine-structure constant within a single experimental setup, with common-mode rejection of certain systematic effects.[42] Calculations indicate that $^{229}Th^{3+}$ shows promise as an ionic clock candidate, capable of achieving 10^{-18}-level accuracy via the 5f $^2F_{5/2}\rightarrow$ 5f $^2F_{7/2}$ electronic transition. Based on this frequency accuracy of $^{229}Th^{3+}$ ionic clock, measuring the frequency ratio between the nuclear and ionic clock could yield a precision of 10^{-21}-yr^{-1} for the drift of the fine structure constant ($\dot{\alpha}/\alpha$). Building on the above advantages of the ionic nuclear clock and our group's established research in this field, this review focus on the current status and prospects of ionic nuclear clocks.

Table 2. Performance comparison of different nuclear optical clock concepts.

	Type	Uncertainty	Stability	Ref.
Ionic	single ion	1.5×10^{-19}	$5\times10^{-16}/\sqrt{\tau}$	[11]
	multiple ion	$>1.5\times10^{-19}$	$5\times10^{-17}/\sqrt{\tau}$	[39]
Solid-state	crystal lattice	$\sim10^{-18}$	$5\times10^{-17}/\sqrt{\tau}$	[36,41]
	internal conversion	7.9×10^{-12}	$2\times10^{-18}/\sqrt{\tau}$	[37]

The first detailed proposal for an ionic nuclear clock was presented by Peik and Tamm in 2003.[10] The trivalent (3+) state was chosen because it has a suitable electron energy level structure that allows for direct laser cooling. Apart from the 3+ state, the monovalent (1+) and divalent (2+) states have received widespread attention. Their abundant electron energy levels provide more possibilities for resonantly enhancing excitation via an electronic bridge process.[43–45] Other charged thorium ions, such as Th^-,[46,47] Th^{4+},[48] Th^{6+},[49] and Th^{35+},[50] have also been investigated. In this paper, $^{229}Th^{n+}$ ions ($n=1, 2, 3$) are reviewed in terms of their generation, trapping, cooling, and the realization of the clock cycle.

2. Generation of the thorium ions

Thorium is a refractory metal with a high melting point (2023 K), making it difficult to produce an atomic source of ^{229}Th. Additionally, the ionization energies of Th, Th^+, Th^{2+}, and Th^{3+} range from several electronvolts to tens of electronvolts, as shown in Table 3. Therefore, producing thorium ions via photoionization is complex. Even for generating Th^+ ions, three-photon resonance photoionization is required.[51] Furthermore, ^{229}Th is an extremely rare radioactive isotope, with an estimated global stock of ~ 40 g at reasonable isotopic purity.[36,52] Given these factors, laser ablation is a relatively suitable method for ion generation. From the perspective of ^{229}Th acquisition, another feasible approach to obtain thorium ions from the α decay of ^{233}U is employed in some research groups. Comparing these two methods, laser ablation is easy to operate but has a low ion yield, while α decay enables continuous ion generation yet requires complex purification. Alternative approaches, such as inductively coupled plasma techniques[53] and electron-beam evaporation,[54] are also under investigation.

Table 3. Ionization thresholds for several thorium ions. The data are obtained from NIST: Atomic Spectra Database – Ionization Energies Form.

Ionic charge	0	1+	2+	3+
Ionization threshold (eV)	6.31	12.10	18.32	28.65
Corresponding wavelength (nm)	196	102	68	43

2.1. Generating thorium ions via laser ablation

Laser ablation uses a short pulse laser with sufficiently high energy density to irradiate the surface of solid targets, inducing rapid heating and phase transitions, thereby generating plasma. At low pulse laser intensities, neutral atoms are predominantly produced during the ablation process[55] and can be further photoionized within an ion trap.[56–59] When the laser pulse intensity is sufficiently high,[60] large numbers of charged ions and electrons are produced during the ablation process.[61–63] For thorium ion generation, when the laser intensity exceeds a threshold on the order of 10^8 W·cm^{-2}, ions escape from the plume (an expanding plasma consisting of various neutral particles, electrons, and ions with diverse charge-to-mass ratios and energy distributions)[64] and move away from the target surface at velocities in the range of 10^4 m·s^{-1}.[65] Additionally, it has been observed that at shorter wavelengths, the transition from thermal ablation to phase explosion occurs at lower laser photon fluences, indicating that the ablation threshold decreases with decreasing laser wavelength.[66–68] To avoid perturbing the electric potential of the ion trap, the ablation target is typically positioned outside the trap.

A ^{232}Th metal target is placed $\sim$ 55 mm away from the entrance endcap along the trap axis, as shown in Fig. 2(a). A diode-pumped pulsed laser at 1064 nm wavelength is used for ablation, with a pulse duration of 8 ns and a pulse energy of 450(30) μJ. It is focused to an 80(10) μm spot size on the target at an incident angle of $\sim 30°$, resulting in a laser intensity of $2.80(72)\times10^8$ W·cm^{-2}. Under these conditions, Th^+, Th^{2+}, and Th^{3+} ions are generated.[69] A 3D Monte Carlo simulation of the dynamic process was performed using SIMION to investigate the velocity distributions of ablated thorium ions.[70] The simulation indicates that the velocity distributions of ablated ions can be described by the shifted Maxwell–Boltzmann–Coulomb (MBC) distribution function[71]

$$F(v) = A\,(m/2\pi kT)^{3/2}\,v^3 \exp\left(-m\,(v-(v_{\rm k}+v_{\rm c}))^2/2kT\right), \quad (1)$$

where A is a normalization constant, kT is the ion distribution temperature, m and v are the ion mass and velocity, $v_{\rm k} = \sqrt{\gamma kT/m}$ is the center-of-mass velocity ($\gamma = 5/3$ for monatomic metal samples), and $v_{\rm c}$ is the Coulomb velocity depending on the magnitude of the effective electric field generated by the plasma. The MBC velocity distributions of various ablated charged thorium ions are illustrated in Fig. 2(b). As the ion charge state increases, the most probable velocity of the ions increases while the proportion of ions decreases. According to the mass spectrum signal shown in Fig. 5(b), the ratio of Th^{3+} ions to Th^+ ions is 18%, and the ratio of Th^{2+} ions to Th^+ ions is 50%. This indicates a lower yield of higher-charge-state ions, as generating such ions involves a smaller ionization cross section and requires higher energy.

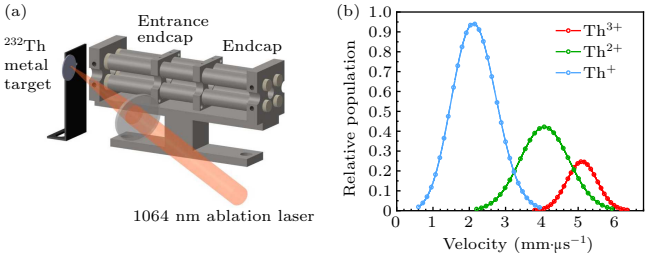


Fig. 2. Generation of thorium ions with different charge states via laser ablation. (a) Schematic diagram of loading ions via laser ablation. A 1064 nm ablation pulse laser is focused on the target, which is positioned in front of the entrance endcap along the trap axis. (b) Velocity distributions of ablated Th^{3+} (red line), Th^{2+} (green line), and Th^+ (blue line) ions, corresponding to the optimal parameters of the shifted Maxwell–Boltzmann–Coulomb distribution.[69]

Table 4. Corresponding parameters and characteristics of thorium ions generated via laser ablation.

Target	Laser wavelength (nm)	Laser intensity (W·cm^{-2})	Aiming ion species	Ref.
^{232}Th metal	355	2.26×10^{10}	Th^{3+}	[72]
^{229,232}Th(NO$_3$)$_4$	355	6.37×10^{9}	Th^{3+}	[73]
^{232}Th metal	337	2.80×10^{8}	Th^+, Th^{2+}	[65]
^{229,232}Th(NO$_3$)$_4$	1064		Th^+	[77]
^{232}Th metal	1064	6.37×10^{9}	Th^+, Th^{2+}, Th^{3+}	[79]
^{232}Th metal	337	1.00×10^{8}	Th^+, Th^{2+}	[81]
^{232}Th metal	1064	2.80×10^{8}	Th^+, Th^{2+}, Th^{3+}	[69]

Such an ablation method has also been successfully implemented at the Georgia Institute of Technology,[72,73] PTB,[65,74–78] Moscow Engineering Physics Institute (MePhI),[53,79,80] and Griffith University.[81] The detailed parameters are summarized in Table 4. Furthermore, laser ablation can also be combined with photoionization[76,77] or electron impact ionization[82] to generate thorium ions.

2.2. Generating thorium ions via α decay of ^{233}U

The ^{229}Th has no natural abundance but can be artificially produced through the decay of parent nuclides. As illustrated in Fig. 3(a), ^{229}Th is populated via three natural decay paths: electron capture decay of ^{229}Pa, β^- decay of ^{229}Ac, and α decay of ^{233}U.[83] For the first pathway, ^{229}Pa absorbs an electron and converts a proton to a neutron, thus generating ^{229}Th with a characteristic half-life of 1.5 days. The major challenge in obtaining ^{229}Th via this decay channel lies in the inherently low production yield of the parent nuclide ^{229}Pa itself. As an alternative, ^{229}Ac undergoes β^- decay to produce ^{229}Th rapidly, with a half-life of 62.7 min. However, ^{229}Ac currently requires production in an online facility, such as the ISOLDE facility at CERN.[84] Regarding the α decay of ^{233}U, this radioactive decay has a half-life of $\sim$ 159200 years. The parent nuclide ^{233}U can be sustainably and stably produced in Th–U molten salt reactors (MSRs).[85] Beyond nuclear decay pathways, ^{229}Th can be produced via the neutron transmutation of ^{226}Ra, ^{228}Ra, ^{227}Ac

and ^{228}Th in reactor-based production.[86,87] Additionally, an alternative approach for ^{229}Th production has been proposed, which involves bombarding a polyethylene (CH_2) target with accelerated ^{232}Th ions to induce the neutron-knockout reaction ($^{232}\text{Th} \rightarrow {}^{229}\text{Th} + 3\text{n}$).[88]

Among these approaches, the α decay of ^{233}U currently represents the only means to obtain usable quantities of ^{229}Th. The decay chain of ^{233}U proceeds through sequential α and β^- decays, as illustrated in Fig. 3(b), ultimately yielding stable ^{209}Bi as the end product. According to the half-life of ^{233}U, its decay constant is determined to be 1.38×10^{-13} s^{-1}. Consequently, it can be calculated that 1000 Bq of ^{233}U corresponds to 7.25×10^{15} atoms, with a mass of approximately 2.8 μg. For ^{229}Th with the same activity level, the corresponding number of atoms and mass are 3.59×10^{14} and 0.137 μg, respectively. The extraction of ^{229}Th from the α decay of a ^{233}U source can continuously produce ^{229}Th ions of varying charge states, with approximately 2% of them populating the isomeric state.[89,90] In 2015, Wense *et al.* quantitatively determined the activities of ^{233}U and its decay daughters using γ-ray energy and α-energy spectra, and evaluated the emission efficiency of α-recoil particles through recoil ion implantation experiments.[91]

The ^{229}Th α-recoil ions leave the source material with a kinetic recoil energy of 84.3 keV, necessitating a high-density buffer-gas environment and thus a complex differential pumping setup. To date, Ludwig–Maximilians–Universität (LMU),[77,91–96] PTB,[97,98] and Rikagaku Kenkyusho (RIKEN)[12] have constructed dedicated setups for thorium ion extraction from the α decay of ^{233}U sources and successfully obtained ^{229}Th ions. The experimental setup at LMU[92] is shown in Fig. 4. The ^{233}U source is mounted in front of a radio-frequency (RF) and direct-current (DC) funnel placed within a buffer-gas stopping cell. ^{229}Th ions, along with other daughter products of the ^{233}U decay chain, are first decelerated in the buffer-gas stopping cell filled with 40 mbar of ultra-pure He 6.0 and then guided by the RF + DC funnel system (comprising 50 ring electrodes) towards a Laval extraction nozzle. Upon passing through the nozzle, the extracted ions are accumulated in a radio-frequency quadrupole (RFQ). Subsequently, a quadrupole mass filter (QMF) is used to select target thorium ions, filtering out thorium ions in other charge states, other decay products, and molecular ions formed via reactions with impurities in the buffer gas. After mass purification of the ion beam, the ions are transported to an ion trap with low kinetic energy. The extraction efficiencies of Th^{3+}, Th^{2+}, and Th^{+} ions are 10%, 5.5% and 0.3%, respectively.[91] At PTB,[97] the thorium ion beam is subsequently bent by 90° via an electrostatic deflector to provide unobstructed laser access along the trap axis. An RF electric octupole guide is used to transport

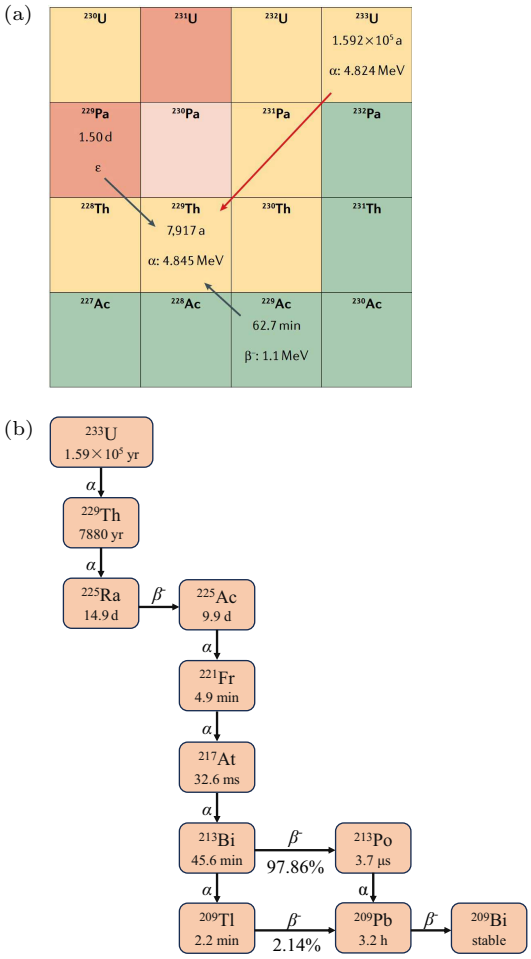


Fig. 3. Generation of ^{229}Th via nuclear decay pathways. (a) A section of the nuclide chart showing the natural decay pathways that lead to the production of ^{229}Th.[83] (b) Decay chain of ^{233}U. The data are obtained from Livechart – Table of Nuclides - Nuclear structure and decay data.

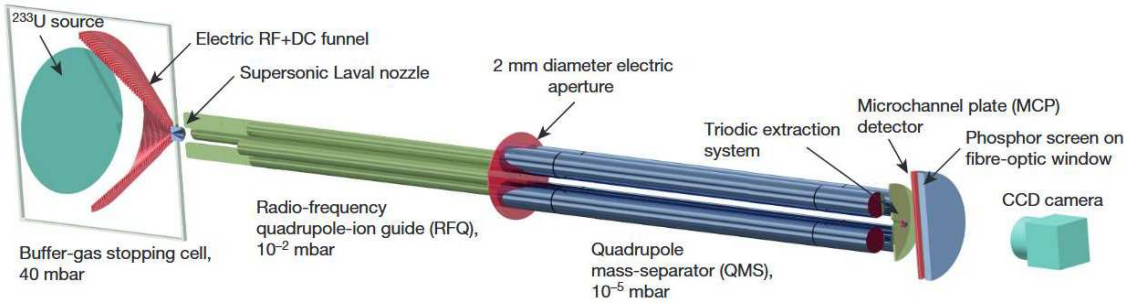


Fig. 4. Schematic of the experimental setup for extracting thorium ions from the α decay of a ^{233}U source at LMU.[92]

the ions from the deflector to the ion trap. In contrast to the setups at LMU and PTB, the extraction process at RIKEN[12] is achieved using an RF carpet located in a vacuum chamber, which is filled with helium buffer gas (20 mbar). The extracted ions are then directly transported to a linear ion trap. The trap chamber is filled with helium buffer gas at a pressure of 2×10^{-3} mbar, eliminating the need for multistage differential pumping.

3. Trapping of thorium ions in ion traps

Since thorium ions produced by laser ablation or α decay of ^{233}U have relatively high velocities, they typically require deceleration and transport from external regions into the trap center for long-term stable confinement, which facilitates the subsequent manipulation for realizing the ionic nuclear optical clock. Trapping of ^{229}Th ions has been achieved at the Georgia Institute of Technology,[73] PTB,[76,77,98] LMU,[77,91] and RIKEN.[12] Additionally, several experiments have reported the successful trapping of ^{232}Th ions.[65,69,72,74,75,78–81]

3.1. Dynamic loading

Ions are commonly loaded into the trap via two approaches: axial injection (along the trap axis) or radial injection (perpendicular to the trap axis). For ablated ions, radial ablation loading exploits co-generated ions and electrons to momentarily neutralize the RF voltage on the trap electrodes, enabling rapid suppression of the confinement barrier within 1 μs.[65] Following ion injection, the RF trapping potential is swiftly restored on a comparable timescale of μs, thereby achieving ion loading. The axial confinement of the ion trap employs a static electric field, which provides superior control precision compared to the RF electric field. Furthermore, axial ablation loading demonstrates an enhanced capacity to trap ions with broader kinetic energy distributions when the distance between the trap center and endcap electrodes increases.[69,99] Currently, following laser ablation, successful ion loading along the radial direction is limited to Th^+ and Th^{2+} ions,[65] while axial loading accommodates Th^+, Th^{2+}, and Th^{3+} ions.[69,79] For thorium ions generated via the α decay of ^{233}U, they are typically injected into the trap along the axial direction after collisional deceleration with buffer gas.[95,97,98]

Compared with passive loading, in which the endcaps remain fixed, the loading efficiency can be dramatically improved via dynamic temporal control of the axial trapping potentials.[100] In order to dynamically load thorium ions from the axial direction, when the ablation laser fires, the voltage on the entrance endcap is switched off within 1 μs and held at 0 V for a period, as shown in the upper panel of Fig. 5(a). Once the ions reach the center of the ion trap, the voltage at the entrance endcap is quickly switched back within 1 μs to realize axial confinement, as depicted in the lower panel of Fig. 5(a). This dynamic laser ablation loading method allows the trapping of not only slow, singly charged ions but also fast, multiply charged ions.

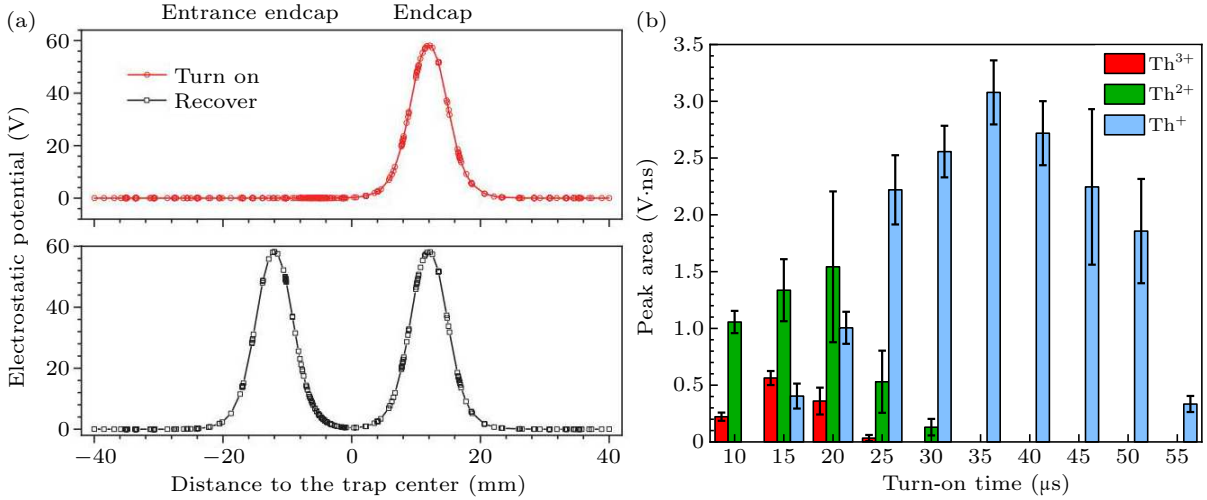


Fig. 5. Dynamic loading. (a) Axial electrostatic potential distribution as a function of distance from the trap center; turn on (in red): the voltage of the entrance endcap is pulsed down from 70 V to 0 V; recovery (in black): the voltage of the entrance endcap is switched back from 0 V to 70 V. Turn-on time of the entrance endcap: the duration for holding 0 V on the entrance endcap.[99] (b) Comparison of the peak areas of Th^{3+} (red bar), Th^{2+} (green bar), and Th^+ (blue bar) ions at different turn-on times in the experiment.[69]

The dynamic ion loading method offers greater controllability compared to directly loading laser ablation-generated ions into an ion trap. In addition to the ion trap's RF voltage, endcap voltage, and buffer gas partial pressure, dynamic loading can also control the number and velocity distribution of loaded ions via the trap's endcap turn-on time.[99] Figure 5(b) illustrates the variation in signal intensity of trapped thorium ions with different charge states as a function of the turn-on time of the entrance endcap, which ranges from 10 μs to 55 μs. Th^{3+}, Th^{2+}, and Th^+ ions achieve optimal loading at 15 μs,

20 μs, and 35 μs, respectively, which correlates with their velocity distributions. Additionally, the total lifetime of trapped $^{232}Th^{3+}$ ions has been measured. In Fig. 6, the black dots show that the fitted total lifetime of Th^{3+} ions in the presence of helium buffer gas is 24(3) s.[69] By further optimizing the RF trapping potential to mitigate RF heating effects and purifying the helium buffer gas, the total lifetime of Th^{3+} ions is significantly extended to 493(32) s, as indicated by the red dots. Under these conditions, laser cooling of Th^{3+} ions becomes experimentally feasible. Replacing the current ion trap with a cryogenic ion trap will significantly extend ion lifetimes, owing to improved vacuum conditions and effective suppression of electromagnetic interference.[95,96,101]

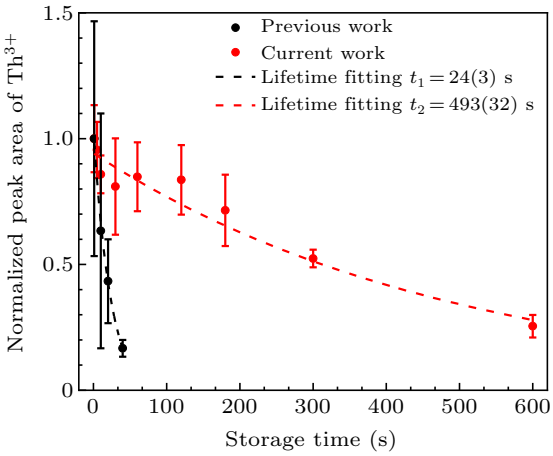


Fig. 6. Total lifetime enhancement of trapped $^{232}Th^{3+}$ ions via optimization of the RF trapping potential and purification of the buffer gas. The black dots show the temporal decay of the Th^{3+} ion signal peak area under pre-optimization conditions[69] and the red dots represent the current result after optimization. The exponential decay curve $y = A \cdot e^{(-t/t_0)}$ is used to fit the peak area of thorium ions, where t_0 is the lifetime.

3.2. Detection of thorium ions via mass spectrometry

Due to the short lifetime of trapped thorium ions and the difficulty of fluorescence detection, existing methods for the initial demonstration of trapped thorium ions primarily rely on mass spectrometry techniques, including quadrupole mass spectrometry (QMS)[92,102,103] and time-of-flight (TOF) mass spectrometry.[65,69,82,104]

As illustrated in Fig. 7(a), the integration of a linear ion trap with a time-of-flight mass spectrometer (LIT TOF-MS) comprises an ion trap, electrostatic lenses, deflection electrodes, and a channel electron multiplier (CEM) detector. Similar to the Wiley–McLaren configuration, the two trap rods farther from the grounded plate serve as repelling rods with a higher positive potential (≈ 1000 V), while the two closer ones act as extracting rods with a lower positive potential (≈ 800 V). Together with the grounded plate, they form a three-stage Wiley–McLaren-type TOF mass spectrometer. Upon exiting the grounded plate, ions enter a field-free drift region where transverse divergence occurs perpendicular to their propagation axis. Two Einzel lenses are used to focus and collimate the ion beam into a compact profile. Additionally, two orthogonally aligned pairs of parallel deflection plates are mounted between the lenses to control the ion beam vertically and horizontally. The focused and deflected ion beam ultimately reaches the CEM detector, where the ion signal is detected.

Ablated thorium ions with different charge states exhibit different velocity distributions, as discussed in Subsection 2.1, and arrive at the trap center with different flight times. A typical mass spectrum of thorium ions at the turn-on time of

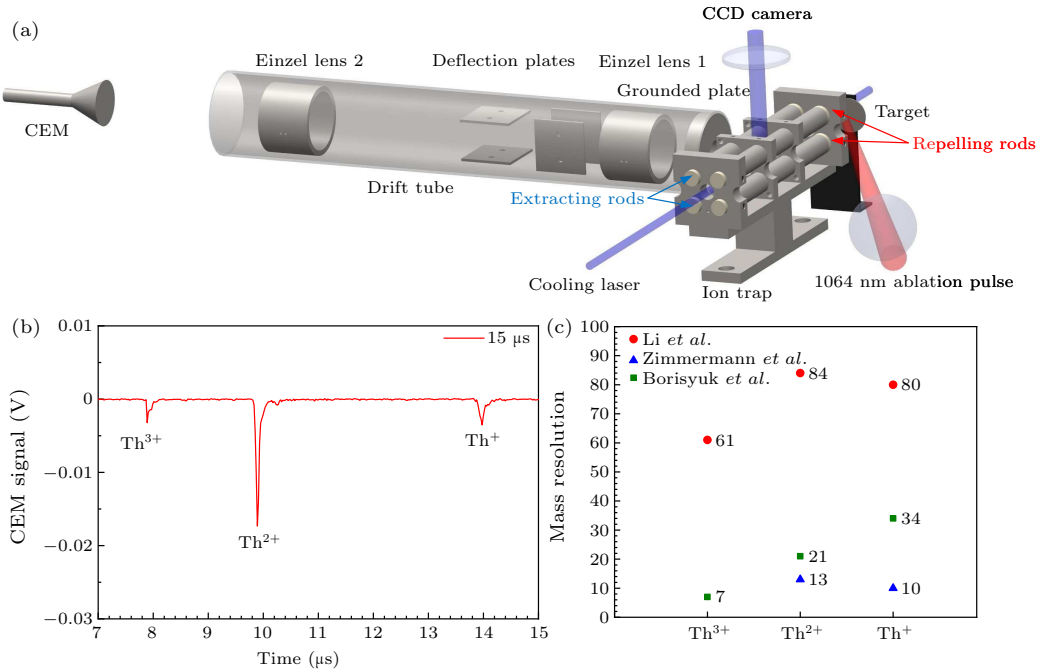


Fig. 7. Mass spectrometry of thorium ions with different charge states.[69] (a) Schematic of the experimental setup. A linear ion trap is integrated with a TOF mass spectrometer. (b) A typical TOF mass spectrum of thorium ions with various charge states at the turn-on time of 15 μs. (c) Mass resolutions of thorium ions mass spectrometry.

15 μs is shown in Fig. 7(b). The full width at half maximum (FWHM) values for Th^{3+}, Th^{2+}, and Th^{+} ions at a turn-on time of 15 μs are 64 ns, 59 ns, and 87 ns, corresponding to mass resolutions of 61, 84, and 80, respectively, for thorium ions mass spectrometry at 300 K. These data (red dot) are presented in Fig. 7(c). Zimmermann *et al*. (blue triangle) employed TOF mass spectrometry to measure the ion yield and the distribution across the charge states of laser-ablated thorium ions. Due to limitations of laser energy density, only mass resolutions of 13 and 10 were obtained for Th^{2+} and Th^{+} ions, respectively.[65] Borisyuk *et al*. (green square) used a multi-sectional quadrupole linear Paul trap with an energy analyzer along the trap axis to measure energy distributions, with mass resolutions of Th^{3+}, Th^{2+}, and Th^{+} ions being 7, 21, and 34, respectively.[79]

Apart from the above works, Churchill *et al.* modified the ion trap by integrating a CEM detector positioned off-axis at one end of the trap for mass spectrometry of thorium ions.[102] Building upon this foundation, Campbell *et al.* constructed a segmented hyperbolic ion trap with high-quality quadrupole potential control, enabling the confinement and mass spectrometric detection of trapped thorium ions.[103] Notably, Groot-Berning *et al*. implemented a dual detection scheme that combines non-destructive identification of trapped thorium ions via Ca^{+} Coulomb crystal fluorescence with destructive TOF analysis, achieving a TOF detection efficiency $> 95\%$ and a mass resolution of $m/\Delta m \approx 500$ for Th^{+}.[82] Telnov *et al*. developed a multi-segment quadrupole ion trap equipped with a secondary electron multiplier (SEM) for thorium ion detection, with TOF mass spectrometry calibrated using $^{88}Sr^{+}$ ions.[104]

4. Cooling of thorium ions

In ion trap experiments, effective cooling of trapped ions enables more stable ion confinement and suppresses Doppler broadening, thereby enhancing measurement precision. Common methods for ion cooling include buffer gas cooling,[105] resistive cooling,[106] direct laser cooling,[107] sympathetic cooling,[108] sideband cooling,[109] and so on. Typically, collisions with buffer gas are used to decelerate thorium ions, ensuring their effective loading. Once the ions are trapped in the ion trap, sympathetic cooling can be employed to further reduce their kinetic energy, enabling long-term stable confinement for subsequent operations. In particular, for Th^{3+} ions, direct laser cooling can also be utilized to achieve ion cooling.

4.1. Buffer gas cooling

Buffer gas cooling is a widely employed technique for cooling atoms, molecules, or ions to cryogenic temperatures.[110–113] It is achieved via collisional energy transfer between target particles and buffer gas particles in a vacuum chamber. The cooling efficiency depends critically on the temperature of buffer gas and the mass ratio of the buffer gas to the target particles, with optimal cooling achieved when $T_{\rm gas}$ is low and the mass ratio $m_{\rm gas}/m_{\rm target}$ is much less than 1.[114] Owing to its low atomic mass (4 amu) and high ionization threshold (~ 24.6 eV), helium is usually the preferred buffer gas.

As discussed in Subsection 2.1, the velocity of thorium ion produced by laser ablation is on the order of 10^3 m·s^{-1}, corresponding to an ion temperature in the range of 10^4–10^5 K. Such high kinetic energy hinders stable confinement within the trapping potential, causing ions to escape from the ion trap. Thus, buffer gas cooling is routinely employed to cool these ions experimentally. Typical buffer gas partial pressures range from 10^{-7} mbar to 10^{-5} mbar,[69,72,73] while pressures on the order of 10^{-3} mbar are occasionally employed for cooling ions to room temperature and depopulating metastable states by collisional quenching.[65,77] Furthermore, when buffer gases are employed to exert a drag force on ions, partial pressures around 10^{-2} mbar are used.[80] Similarly, thorium ions produced via the α decay channel of ^{233}U decay carry a recoil energy of 84.3 keV, requiring higher buffer gas pressures for effectively decelerating ions, typically on the order of tens of mbar.[12,91,97]

4.2. Direct laser cooling

Laser cooling plays a significant role in modern physics, having advanced the fields of atomic physics,[115] quantum science,[116,117] and precision measurements.[13,118,119] Typically, a cycling transition, in which the ion can continuously absorb and emit photons, is preferred. Among all thorium charge states, the Th^{3+} ion, characterized by a Fr-like electronic configuration with a closed inner shell and one valence electron, is currently the only one that can be directly laser-cooled.

The energy level diagram of the $^{229}Th^{3+}$ ion is given in Fig. 8(a), including the nuclear levels for the clock transition as well as the electronic levels for direct laser cooling. The laser cooling process is divided into two steps. In the first step, the two-level transition from 5f $^2F_{5/2}$ state to 6d $^2D_{3/2}$ state (green arrow) is used for laser cooling, at a laser wavelength of 1088 nm. In the second step, further cooling is achieved using a Λ-type three-level system formed by the 5f $^2F_{5/2}$, 6d $^2D_{5/2}$ and 5f $^2F_{7/2}$ states, requiring wavelengths of 690 nm (pink arrow) and 984 nm (orange arrow).

Due to its lack of hyperfine structure, lower radioactivity, and good material availability, the $^{232}Th^{3+}$ ion was chosen for the initial feasibility demonstration. Direct laser cooling of $^{232}Th^{3+}$ was experimentally achieved in 2009.[72] Subsequently, $^{229}Th^{3+}$ ion was also successfully laser cooled in 2011 and the isotope shifts of several electronic transitions be-

tween $^{229}Th^{3+}$ and $^{232}Th^{3+}$ were estimated,[73] as shown in the second column of Table 5. Additionally, the isomer shift of the $5F_{5/2} \leftrightarrow 6D_{3/2}$ transition (1088 nm) was measured by Yamaguchi *et al.*,[12] as illustrated in the third column of Table 5.

For the $^{229}Th^{3+}$ ion, the nuclear ground state has a nuclear spin of 5/2 and the nuclear isomeric state has a nuclear spin of 3/2, resulting in the hyperfine level splitting. The corresponding hyperfine energy splittings are also illustrated in Fig. 8(a). The energy shifts arising from the hyperfine structure in $^{229}Th^{3+}$ are on the order of GHz. These shifts can be addressed using electro-optic modulators (EOMs), thus achieving laser pumping of the hyperfine structure. An image of $^{229}Th^{3+}$–$^{232}Th^{3+}$ bi-component Coulomb crystal is shown in Fig. 8(b).[73] The top image was taken with both $^{229}Th^{3+}$ and $^{232}Th^{3+}$ 690 nm fields present. The $^{232}Th^{3+}$ and $^{229}Th^{3+}$ 690 nm fields were then removed for the middle and bottom images, respectively. The larger mass-to-charge ratio of $^{232}Th^{3+}$ causes it to radially accumulate in the outer shells of the crystal.

Table 5. Measured relative isotope shifts between $^{229}Th^{3+}$ and $^{232}Th^{3+}$ and isomer shifts between $^{229m}Th^{3+}$ and $^{229g}Th^{3+}$.

Transition	Isotope shift (MHz)	Isomer shift (MHz)
	Ref. [73]	Ref. [12]
$5F_{5/2} \leftrightarrow 6D_{3/2}$	−9856(10)	320(30)
$5F_{5/2} \leftrightarrow 6D_{5/2}$	−10509(7)	
$5F_{7/2} \leftrightarrow 6D_{5/2}$	−9890(9)	

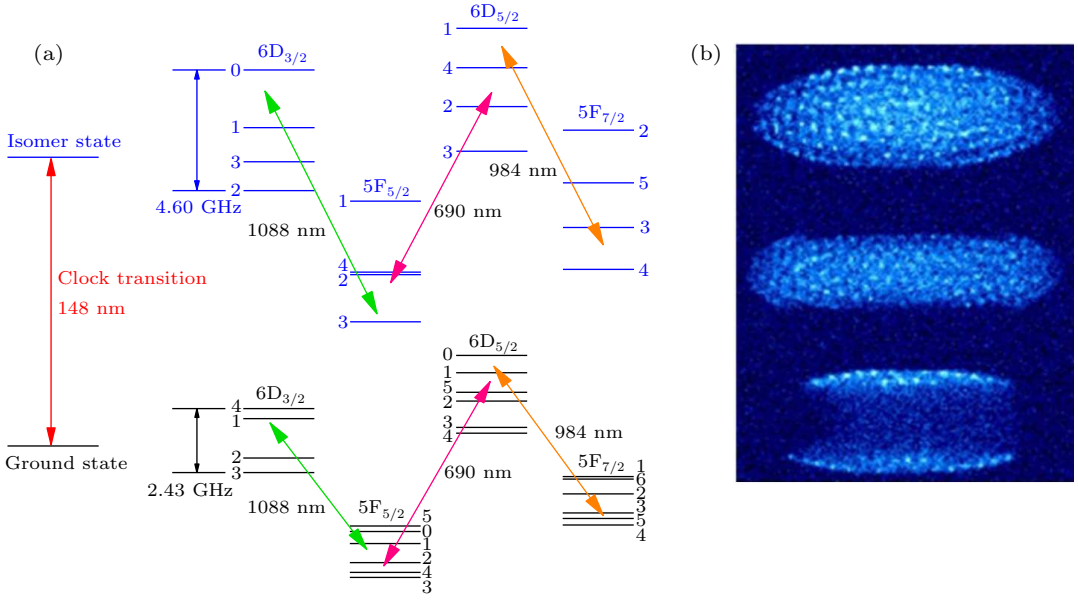


Fig. 8. Direct laser cooling of Th^{3+} ions. (a) Energy level diagram of the $^{229}Th^{3+}$ ion. The left panel shows the nuclear states involved in the clock transition, which is indicated by a red arrow. The right panel presents the hyperfine electronic level structure of $^{229}Th^{3+}$ employed for direct laser cooling. The upper levels (blue solid lines) correspond to the electronic energy levels when the nucleus is in the isomer state, while the lower levels (black solid lines) correspond to the electronic structure with the nucleus in the ground state. (b) Trapped $^{229}Th^{3+}$ and $^{232}Th^{3+}$ ions, laser cooled to crystallization.[73] The images (from top to bottom) were captured with both $^{229}Th^{3+}$ and $^{232}Th^{3+}$ 690 nm fields active, only the $^{229}Th^{3+}$ 690 nm field active, and only the $^{232}Th^{3+}$ 690 nm field active.

4.3. Sympathetic cooling

For atomic or molecular ions that cannot be directly laser-cooled, sympathetic cooling presents an essential methodology to reach ultracold regimes. This technique is achieved by co-confining laser-cooled ions and target ions within the same ion trap, where target ions are cooled via energy transfer to the laser-cooled ions through Coulomb interactions. The minimum temperature achievable through sympathetic cooling is constrained by the cooling limit of the laser-cooled ions and the interaction strength between the two ion species.

In bi-component Coulomb crystals, ions with different mass-to-charge ratios exhibit radial separation. The radius of the ionic motion region and the ion's mass-to-charge ratio satisfy the formula $r_1/r_2 = \sqrt{M_1/Q_1}/\sqrt{M_2/Q_2}$,[120] where r_1 and r_2 are the radii of the motion regions of the ions with the mass-to-charge ratio M_1/Q_1 and M_2/Q_2, respectively. Therefore, ions with higher mass-to-charge ratios experience weaker radial confinement forces, positioning them in the outer regions of the crystal, while those with lower mass-to-charge ratios are more strongly confined and localized near the central regions. When ions have closely matched mass-to-charge ratios, their close spatial proximity enhances Coulomb interactions, leading to improved sympathetic cooling efficiency through stronger coupling of collective motions.

To effectively sympathetically cool thorium ions, the mass-to-charge ratio of the laser-cooled ions should be close to that of the target thorium ions. In 2019, Groot-Berning *et al.* successfully loaded and trapped a $^{232}Th^{+}$ ion in a linear Paul trap, which was embedded in and sympathetically cooled by small crystals of trapped $^{40}Ca^{+}$ ions.[82] PTB demonstrated

the first realization of sympathetic cooling between $^{230}Th^{3+}$ and $^{88}Sr^{+}$ ions, achieving the formation of a two-component Coulomb crystal.[97] Building on this foundation, the hyperfine structure of $^{229}Th^{3+}$ ions in the nuclear ground state has recently been investigated via laser spectroscopy of trapped $^{229}Th^{3+}$ ions that are sympathetically cooled by laser-cooled $^{88}Sr^{+}$ ions in a linear Paul trap.[98]

In our laboratory, $^{88}Sr^{+}$ and $^{232}Th^{3+}$ ions generated via laser ablation of a mixed target are loaded into a linear ion trap. Laser-cooled $^{88}Sr^{+}$ ions produce bright fluorescence, forming a multi-component Coulomb crystal with dark $^{232}Th^{3+}$ ions. Ejecting the crystal yields a TOF mass spectrum with distinct peaks corresponding to $^{88}Sr^{+}$, $^{88}SrO^{+}$, and $^{232}Th^{3+}$ ions, confirming the successful sympathetic cooling of $^{232}Th^{3+}$ ions by the co-trapped $^{88}Sr^{+}$ ions.[121]

5. Realization of a closed-loop clock cycle in thorium nuclear optical clock

In contrast to conventional atomic clocks, where closed-loop clock cycles rely on electronic transitions with accessible excitation pathways and fast spontaneous decay, the realization of a closed-loop cycle in the ^{229}Th nuclear optical clock faces unique and formidable challenges. The nuclear transition in ^{229}Th involves an extremely narrow linewidth and a radiative lifetime of $\sim 10^3$ s,[12] posing significant obstacles to both efficient excitation and fast deexcitation. This section summarizes current strategies for nuclear excitation and recent advances in nuclear isomer quenching.

5.1. Isomer excitation

Since the second nuclear excited state has an energy of 28.4 keV, which is significantly higher than that of the first excited state, the nucleus can be approximated as a closed two-level system consisting of the nuclear ground state $|g\rangle$ and the first nuclear excited state $|e\rangle$ for theoretical calculations of the direct nuclear transition probability in ^{229}Th. The time-dependent nuclear excitation probability $\rho_{\rm exc}(t)$ for a single nucleus under resonant irradiation is given by Torrey's solution to the optical Bloch equations.[122] The Rabi frequency between the isomeric state and the nuclear ground state is

$$\Omega_{\rm eg} = \sqrt{\frac{2\pi c^2 I C_{\rm eg}^2 \Gamma}{\hbar w_{\rm nuc}^3}}. \tag{2}$$

Here, I represents the intensity of the excitation laser, $w_{\rm nuc}$ is the angular frequency of the nuclear transition, $\hbar$ denotes the reduced Planck constant, c is the velocity of light and Γ corresponds to the linewidth of the isomeric state. The Clebsch–Gordan coefficient for the sub-state transition between the isomeric state and the nuclear ground state $C_{\rm eg}$ is 1.[123] Based on the above calculation, Li *et al*. considered the relationship between the laser linewidth $\Gamma_{\rm L}$ and the Doppler broadening linewidth $\Gamma_{\rm D}$ and obtained the modified Rabi frequency.[124]

So far, VUV pulse lasers generated via four-wave mixing (FWM)[33,34,36,125–127] and VUV frequency comb[35,41] have been used to irradiate different ^{229}Th-doped crystals, achieving direct nuclear excitation of ^{229}Th. Most recently, continuous wave (CW) VUV laser sources at 148 nm have also been demonstrated, which are obtained via two distinct approaches: second-harmonic generation (SHG) in a randomly quasi-phase matched SrB_4O_7 crystal[128] and FWM in cadmium vapor.[129] The detailed parameters are listed in Table 6. A power spectral density on the order of femtowatts per hertz (fW·Hz^{-1}) is sufficient to successfully excite ^{229}Th in ^{229}Th-doped crystals from its nuclear ground state to the nuclear isomeric state. However, the particle density in Coulomb crystals ($\sim 10^8$ cm^{-3} [130,131]) is seven to ten orders of magnitude lower than that in thorium-doped crystals (10^{15}–10^{18} cm^{-3} [32,34,40]), resulting in a corresponding reduction in signal intensity. Therefore, to achieve direct nuclear excitation in ion systems, the development of high-power, narrow-linewidth CW VUV laser sources is still necessary. Notably, the power spectral density of the latest VUV CW laser can reach nanowatts per hertz (nW·Hz^{-1}), which is approximately 4 to 6 orders of magnitude higher than that of previous work, making the direct nuclear excitation of ion systems feasible.

Beyond direct nuclear excitation, alternative excitation channels are under investigation, among which electronic bridge (EB) excitation has attracted significant attention. The EB excitation can be effectively treated as a process where an electron, when absorbing the energy of single photon, undergoes a transition from an initial state to a virtual intermediate state and then to a final state. At the same time, the nucleus is excited to the isomeric state from its ground state. Importantly, the resonance condition must be fulfilled. The energy difference between the virtual intermediate state and the final electronic state has to match the nuclear transition energy. The EB process of thorium ions with different charge states is discussed, including Th^{+},[43,44] Th^{3+},[133–135] Th^{4+},[48] Th^{6+},[49] and Th^{35+}[50] ions. In 2024, Wang *et al.* accounted for both hyperfine structure and atomic decay of electronically excited ions, and their calculation results demonstrated that a remarkable 99.7% isomeric population transfer was theoretically reached via the stimulated Raman adiabatic passage method, presenting a potential nuclear-laser scheme based on the EB mechanism.[136] Beyond direct nuclear excitation and EB excitation, other isomeric excitation schemes are under discussion, including nuclear excitation by electron capture (NEEC) in plasma[137,138] or at heavy ion storage rings,[88,139] and the nuclear excitation via laser-driven electron recollision.[140,141]

Table 6. Detailed parameters of different VUV laser sources at 148 nm.

	Type	Power	Linewidth	Power spectral density	Pump source
Pulsed laser	FWH in Xe gas[126]	0.81 mW	≤ 6 GHz	135 fW·Hz^{-1}	249.6 nm; 90 mW 765–800 nm; 480 mW
	FWH in Xe gas[33]	0.45 mW	≤ 10 GHz	45 fW·Hz^{-1}	
	FWH in Xe gas[127]	300 μW	< 6 GHz	50 fW·Hz^{-1}	249.63 nm 420–800 nm
	FWH in Xe gas[34,36]	30–60 μW	10–15 GHz	2–6 fW·Hz^{-1}	
	FWH in Xe gas[125]	5 μW	30 MHz	167 fW·Hz^{-1}	250 nm 786 nm; 45–60 mW
	Frequency comb[35,41,132]	1 nW	300 kHz	3.3 fW·Hz^{-1}	1038 nm; 5–7 kW
CW laser	SHG in SrB_4O_7[128]	$1.3^{+0.7}_{-0.6}$ nW	$\sim$ kHz	~ 100 fW·Hz^{-1}	296.8 nm; 325 mW
	FWH in Cd vapor[129]	100 nW	< 100 Hz	1 nW·Hz^{-1}	375 nm; 2 W 710 nm; 4 W

5.2. Isomer deexcitation

^{229m}Th decays to the nuclear ground state through both magnetic dipole (M1) and electric quadrupole (E2) transitions, with the M1 transition being dominant. According to the latest experimental results, the radiative lifetime of the isomer state is $\sim 10^3$ s.[12] This relatively long lifetime results in an extremely slow relaxation process, making it difficult to maintain the stable and continuous oscillation required for the clock, thereby limiting the clock's performance and practical application prospects. Therefore, there is an urgent demand to explore new quenching channels to significantly accelerate isomer deexcitation.

One approach is to exploit the interaction between the ^{229}Th nucleus and its surrounding environment in ^{229}Th-doped crystals. Embedding ^{229}Th ions in specific host crystals may induce changes in nuclear decay properties through crystal electric field effects, potentially accelerating the decay process. A new competing electric-dipole (E1) channel for nuclear decay in a solid-state environment has been identified in Ref. [34]. Furthermore, the induced quenching of the nuclear isomeric state has been experimentally observed in ^{229}Th-doped crystals. In 2024, the isomer half-life was significantly reduced under x-ray beam irradiation, suggesting the existence of additional decay paths.[31] Subsequently, laser induced quenching was observed independently by Schaden *et al.*[142] and Terhune *et al.*[143] The underlying physical process remains unclear and has become a focus of further investigation. Possible candidate mechanisms include couplings to electronic near-bandgap or defect states, EB processes in the electron cascades following X-ray-induced core-electron ionization,[31] or an IC decay process either by resonantly exciting defect-state electrons to the conduction band[143] or by resonantly transferring the $w_{\rm nuc} \approx 8.4$ eV energy to a particle–hole electronic excitation.[144] Recent research has demonstrated that the excited nucleus in a thin ThO_2 sample can decay rapidly by internal conversion. This process reduces the isomeric state lifetime to only ~ 10 μs, allowing $\sim 10^8$ relative reduction in clock interrogation time. A conversion-electron-based nuclear clock could lead to a $\sim 10^4$ improvement in clock instability.[37]

All reported advances in nuclear isomer quenching have been achieved in ^{229}Th-doped crystal systems. For ion trap systems, realizing rapid nuclear isomer quenching mainly relies on the potential of non-radiative channels, such as IC and EB processes. If these non-radiative channels can be enhanced, they might provide alternative pathways for the isomeric state to decay efficiently. Therefore, exploring enhanced IC or EB channels in thorium ions of various charge states will be a key focus.

6. Conclusion

Since the inference of a low-energy nuclear state in ^{229}Th from the α decay of ^{233}U in 1976, this isotope has continued to attract significant research attention. Over the past decades, substantial progress has been made, including advancements toward the realization of the nuclear optical clock. These advancements include, but are not limited to: the proposals of practical ^{229}Th-based nuclear clock schemes, precise determination of the isomeric state energy, direct laser cooling or sympathetic cooling of Th^{3+} ions in Paul traps, measurements of nuclear properties such as magnetic dipole and electric quadrupole moments, and the successful demonstration of direct nuclear excitation.

In this article, we have outlined the essential steps toward realizing an ionic nuclear clock based on ^{229}Th ions confined in a linear ion trap. Starting from the generation of thorium ions via laser ablation and α decay of ^{233}U, to the successful trapping and mass-resolved identification of various charge states, a feasible path for preparing suitable ion samples has been established. Cooling methods including buffer gas cooling, direct laser cooling, and sympathetic cooling have been discussed, each playing a critical role in reducing the motional energy of ions and enabling precision spectroscopy. Furthermore, the core challenge in realizing the ^{229}Th nuclear opti-

cal clock — establishing an efficient closed-loop clock cycle — has been summarized and analyzed. Despite recent experimental and theoretical progress, particularly in crystal systems, many open questions remain for ion-trap platforms, especially regarding efficient excitation under low-density conditions and rapid quenching of the long-lived isomeric state.

Advancing control over nuclear-electronic coupling, improving VUV laser technologies, and exploring enhanced non-radiative decay mechanisms of the nuclear isomeric state will be pivotal for the development of the ^{229}Th ionic nuclear optical clock with unprecedented stability and accuracy, which holds great promise not only for timekeeping, but also for fundamental physics research. The ultimate realization of the ^{229}Th nuclear clock will represent a transformative advancement in optical clock technology by shifting the fundamental reference from electronic to nuclear transitions. It will further open new avenues for probing fundamental physics, allowing ultra-precise investigations of physical constants, searches for temporal variations in the fine-structure constant, and rigorous tests of physics beyond the Standard Model. Such developments are poised to provide unprecedented insights into the fundamental principles that govern our universe.[145] Moreover, coherent control over the nuclear ground state and nuclear isomeric state of ^{229}Th could potentially enable a novel qubit system. This would expand the range of existing qubit carriers beyond ions, which is of great significance for quantum computing and quantum information.[146]

Acknowledgments

Project supported by the Strategic Priority Research Program of the Chinese Academy of Sciences (Grant No. XDB0920000) and the National Natural Science Foundation of China (Grant No. 12341401).

References

[1] McGrew W F, Zhang X, Fasano R J, Schäffer S A, Beloy K, Nicolodi D, Brown R C, Hinkley N, Milani G, Schioppo M, Yoon T H and Ludlow A D 2018 *Nature* **564** 87
[2] Wang D, Guo R, Xiao S, Xin J, Tang T and Yuan Y 2019 *Adv. Space Res.* **63** 2889
[3] Hollberg L 2020 *Position, Navigation, and Timing Technologies in the 21st Century: Integrated Satellite Navigation, Sensor Systems, and Civil Applications* (Chichester: John Wiley & Sons) p. 1497
[4] Liu H, Zhang R, Liu J and Zhang M 2016 *Sci. China Technol. Sci.* **59** 9
[5] Lodewyck J 2019 *Metrologia* **56** 055009
[6] Dimarcq N, Gertsvolf M, Mileti G, *et al.* 2024 *Metrologia* **61** 012001
[7] Kolkowitz S, Pikovski I, Langellier N, Lukin M D, Walsworth R L and Ye J 2016 *Phys. Rev. D* **94** 124043
[8] Safronova M S, Budker D, DeMille D, Kimball D F J, Derevianko A and Clark C W 2018 *Rev. Mod. Phys.* **90** 025008
[9] Bothwell T, Kennedy C J, Aeppli A, Kedar D, Robinson J M, Oelker E, Staron A and Ye J 2022 *Nature* **602** 420
[10] Peik E and Tamm C 2003 *Europhys. Lett.* **61** 181
[11] Campbell C J, Radnaev A G, Kuzmich A, Dzuba V A, Flambaum V V and Derevianko A 2012 *Phys. Rev. Lett.* **108** 120802
[12] Yamaguchi A, Shigekawa Y, Haba H, Kikunaga H, Shirasaki K, Wada M and Katori H 2024 *Nature* **629** 62
[13] Aeppli A, Kim K, Warfield W, Safronova M S and Ye J 2024 *Phys. Rev. Lett.* **133** 023401
[14] Marshall M C, Castillo D A R, Arthur-Dworschack W J, Aeppli A, Kim K, Lee D, Warfield W, Hinrichs J, Nardelli N V, Fortier T M, Ye J, Leibrandt D R and Hume D B 2025 *Phys. Rev. Lett.* **135** 033201
[15] Zhang B, Ma Z, Huang Y, Han H, Hu R, Wang Y, Zhang H, Tang L, Shi T, Guan H and Gao K 2025 arXiv:2506.17423 [physics.atom-ph]
[16] Flambaum V V 2006 *Phys. Rev. Lett.* **97** 092502
[17] Berengut J C and Flambaum V V 2010 *Nucl. Phys. News* **20** 19
[18] Flambaum V V 2019 *Phys. Rev. C* **99** 035501
[19] Wcisło P, Morzyński P, Bober M, Cygan A, Lisak D, Ciuryło R and Zawada M 2016 *Nat. Astron.* **1** 0009
[20] Thirolf P G, Seiferle B and Von Der Wense L 2019 *Ann. Phys. (Berl.)* **531** 1800381
[21] Kroger L A and Reich C W 1976 *Nucl. Phys. A* **259** 29
[22] Reich C W and Helmer R G 1990 *Phys. Rev. Lett.* **64** 271
[23] Helmer R G and Reich C W 1994 *Phys. Rev. C* **49** 1845
[24] Guimarães-Filho Z O and Helene O 2005 *Phys. Rev. C* **71** 044303
[25] Beck B R, Becker J A, Beiersdorfer P, Brown G V, Moody K J, Wilhelmy J B, Porter F S, Kilbourne C A and Kelley R L 2007 *Phys. Rev. Lett.* **98** 142501
[26] Beck B R, Becker J A, Beiersdorfer P, Brown G V, Moody K J, Wu C Y, Wilhelmy J B, Porter F S, Kilbourne C A and Kelley R L 2009 *LLNL-PROC* 415170
[27] Yamaguchi A, Muramatsu H, Hayashi T, Yuasa N, Nakamura K, Takimoto M, Haba H, Konashi K, Watanabe M, Kikunaga H, Maehata K, Yamasaki N Y and Mitsuda K 2019 *Phys. Rev. Lett.* **123** 222501
[28] Sikorsky T, Geist J, Hengstler D, Kempf S, Gastaldo L, Enss C, Mokry C, Runke J, Düllmann C E, Wobrauschek P, Beeks K, Rosecker V, Sterba J H, Kazakov G, Schumm T and Fleischmann A 2020 *Phys. Rev. Lett.* **125** 142503
[29] Seiferle B, Von Der Wense L, Bilous P V, Amersdorffer I, Lemell C, Libisch F, Stellmer S, Schumm T, Düllmann C E, Pálffy A and Thirolf P G 2019 *Nature* **573** 243
[30] Kraemer S, Moens J, Athanasakis-Kaklamanakis M, *et al.* 2023 *Nature* **617** 706
[31] Hiraki T, Okai K, Bartokos M, *et al.* 2024 *Nat. Commun.* **15** 5536
[32] Beeks K, Sikorsky T, Rosecker V, Pressler M, Schaden F, Werban D, Hosseini N, Rudischer L, Schneider F, Berwian P, Friedrich J, Hainz D, Welch J, Sterba J H, Kazakov G and Schumm T 2023 *Sci. Rep.* **13** 3897
[33] Tiedau J, Okhapkin M V, Zhang K, Thielking J, Zitzer G, Peik E, Schaden F, Pronebner T, Morawetz I, De Col L T, Schneider F, Leitner A, Pressler M, Kazakov G A, Beeks K, Sikorsky T and Schumm T 2024 *Phys. Rev. Lett.* **132** 182501
[34] Elwell R, Schneider C, Jeet J, Terhune J E S, Morgan H W T, Alexandrova A N, Tran Tan H B, Derevianko A and Hudson E R 2024 *Phys. Rev. Lett.* **133** 013201
[35] Zhang C, Ooi T, Higgins J S, Doyle J F, Von Der Wense L, Beeks K, Leitner A, Kazakov G A, Li P, Thirolf P G, Schumm T and Ye J 2024 *Nature* **633** 63
[36] Zhang C, Von Der Wense L, Doyle J F, Higgins J S, Ooi T, Friebel H U, Ye J, Elwell R, Terhune J E S, Morgan H W T, Alexandrova A N, Tran Tan H B, Derevianko A and Hudson E R 2024 *Nature* **636** 603
[37] Elwell R, Terhune J E S, Schneider C, Morgan H W T, Tan H B T, Perera U C, Rehn D A, Alfonso M C, Von Der Wense L, Seiferle B,Scharl K, Thirolf P G, Derevianko A and Hudson E R 2025 *Nature* **648** 300
[38] Si R, Shi C, Xue N, Kong X, Chen C, Tu B and Ma Y G 2025 *Sci. China Phys. Mech. Astron.* **68** 272011
[39] Von Der Wense L and Seiferle B 2020 *Eur. Phys. J. A* **56** 277
[40] Beeks K, Sikorsky T, Schaden F, Pressler M, Schneider F, Koch B N, Pronebner T, Werban D, Hosseini N, Kazakov G, Welch J, Sterba J H, Kraus F and Schumm T 2024 *Phys. Rev. B* **109** 094111
[41] Higgins J S, Ooi T, Doyle J F, Zhang C, Ye J, Beeks K, Sikorsky T and Schumm T 2025 *Phys. Rev. Lett.* **134** 113801
[42] Yu S C, Gan W T, Hua X, Tong X and Li C B 2024 *Phys. Rev. A* **109** 063115
[43] Porsev S G and Flambaum V V 2010 *Phys. Rev. A* **81** 042516
[44] Porsev S G, Flambaum V V, Peik E and Tamm C 2010 *Phys. Rev. Lett.* **105** 182501
[45] Safronova M S, Safronova U I and Clark C W 2014 *Phys. Rev. A* **90** 032512
[46] Zhang R, Lu Y, Yan S and Ning C 2025 *Phys. Rev. A* **111** 023102

[47] Tang R, Si R, Fei Z, Fu X, Lu Y, Brage T, Liu H, Chen C and Ning C 2021 *Phys. Rev. A* **103** 042817

[48] Nickerson B S, Pimon M, Bilous P V, Gugler J, Beeks K, Sikorsky T, Mohn P, Schumm T and Pálffy A 2020 *Phys. Rev. Lett.* **125** 032501

[49] Yu S C, Hua X, Tong X and Li C B 2025 *Chin. Phys. Lett.* **42** 120302

[50] Porsev S G, Cheung C and Safronova M S 2021 *Quantum Sci. Technol.* **6** 034014

[51] Raeder S, Sonnenschein V, Gottwald T, Moore I D, Reponen M, Rothe S, Trautmann N and Wendt K 2011 *J. Phys. B: At. Mol. Opt. Phys.* **44** 165005

[52] U. S. department of Energy (accessed on 28 August 2025)

[53] Troyan V I, Borisyuk P V, Khalitov R R, Krasavin A V, Lebedinskii Y Y, Palchikov V G, Poteshin S S, Sysoev A A and Yakovlev V P 2013 *Laser Phys. Lett.* **10** 105301

[54] Troyan V I, Borisyuk P V, Vasil'ev O S, Krasavin A V, Poteshin S S, Sysoev A A, Chernyshev D M, Donchenko S I and Pal'chikov V G 2014 *Meas. Tech.* **57** 777

[55] De Matos J B, Destro M G, Da Silveira C A B and Rodrigues N A S 2014 *Rev. Sci. Instrum.* **85** 083505

[56] Shao H, Wang M, Zeng M, Guan H and Gao K 2018 *J. Phys. Commun.* **2** 095019

[57] Vrijsen G, Aikyo Y, Spivey R F, Inlek I V and Kim J 2019 *Opt. Express* **27** 33907

[58] White B M, Low P J, De Sereville Y, Day M L, Greenberg N, Rademacher R and Senko C 2022 *Phys. Rev. A* **105** 033102

[59] Osada A and Noguchi A 2022 *J. Phys. Commun.* **6** 015007

[60] Stafe M, Marcu A and Puscas N N 2014 *Pulsed Laser Ablation of Solids: Basics, Theory and Applications* (Vol. 53) (Berlin, Heidelberg: Springer)

[61] Kwong V H S 1989 *Phys. Rev. A* **39** 4451

[62] Olmschenk S and Becker P 2017 *Appl. Phys. B* **123** 99

[63] Sameed M, Maxwell D and Madsen N 2020 *New J. Phys.* **22** 013009

[64] Láska L, Jungwirth K, Králikov B, Krása J, Pfeifer M, Rohlena K, Skása J, Ullschmied J, Badziak J, Parys P, Wolowski J, Woryna E, Gammino S, Torrisi L, Boody F P and Hora H 2003 *Plasma Phys. Control. Fusion* **45** 585

[65] Zimmermann K, Okhapkin M V, Herrera-Sancho O A and Peik E 2012 *Appl. Phys. B* **107** 883

[66] Torrisi L, Gammino S, Andò L, Nassisi V, Doria D and Pedone A 2003 *Appl. Surf. Sci.* **210** 262

[67] Hoffman J, Chrzanowska J, Kucharski S, Moscicki T, Mihailescu I N, Ristoscu C and Szymanski Z 2014 *Appl. Phys. A* **117** 395

[68] Prada-Rodrigo J, Maio Y, Faure N, Kachan E, Colombier J P and Sedao X 2024 *J. Laser Micro-Nanoeng.* **19** 179

[69] Li Z, Li L, Hua X and Tong X 2024 *J. Appl.Phys.* **135** 144402

[70] Li L 2024 *The Study on the Preparation and Trapping of Thorium Triply Charged Ions for the Realization of the Nuclear Transition via Electronic Bridge Excitation* (Ph. D. Dissertation) (Wuhan: Innovation Academy for Precision Measurement Science and Technology, Chinese Academy of Sciences) (in Chinese)

[71] Apiñániz J I, Sierra B, Martínez R, Longarte A, Redondo C and Castaño F 2008 *J. Phys. Chem. C* **112** 16556

[72] Campbell C J, Steele A V, Churchill L R, DePalatis M V, Naylor D E, Matsukevich D N, Kuzmich A and Chapman M S 2009 *Phys. Rev. Lett.* **102** 233004

[73] Campbell C J, Radnaev A G and Kuzmich A 2011 *Phys. Rev. Lett.* **106** 223001

[74] Herrera-Sancho O A, Okhapkin M V, Zimmermann K, Tamm Chr, Peik E, Taichenachev A V, Yudin V I and Głowacki P 2012 *Phys. Rev. A* **85** 033402

[75] Herrera-Sancho O A, Nemitz N, Okhapkin M V and Peik E 2013 *Phys. Rev. A* **88** 012512

[76] Okhapkin M V, Meier D M, Peik E, Safronova M S, Kozlov M G and Porsev S G 2015 *Phys. Rev. A* **92** 020503

[77] Thielking J, Okhapkin M V, Głowacki P, Meier D M, Von Der Wense L, Seiferle B, Düllmann C E, Thirolf P G and Peik E 2018 *Nature* **556** 321

[78] Meier D M, Thielking J, Głowacki P, Okhapkin M V, Müller R A, Surzhykov A and Peik E 2019 *Phys. Rev. A* **99** 052514

[79] Borisyuk P V, Derevyashkin S P, Khabarova K Y, Kolachevsky N N, Lebedinsky Y Y, Poteshin S S, Sysoev A A, Tkalya E V, Tregubov D O, Troyan V I, Vasiliev O S, Yakovlev V P and Yudin V I 2017 *Eur. J. Mass Spectrom.* **23** 146

[80] Derevyashkin S P, Borisyuk P V, Khabarova K Y, Kolachevsky N N, Strelkin S A, Tkalya E V, Tregubov D O, Tronin I V and Yakovlev V P 2021 *Laser Phys. Lett.* **18** 015501

[81] Piotrowski M, Scarabel J, Lobino M, Streed E and Gensemer S 2020 *OSA Contin.* **3** 2210

[82] Groot-Berning K, Stopp F, Jacob G, Budker D, Haas R, Renisch D, Runke J, Thörle-Pospiech P, Düllmann C E and Schmidt-Kaler F 2019 *Phys. Rev. A* **99** 023420

[83] Beeks K, Sikorsky T, Schumm T, Thielking J, Okhapkin M V and Peik E 2021 *Nat. Rev. Phys.* **3** 238

[84] Verlinde M, Kraemer S, Moens J, *et al.* 2019 *Phys. Rev. C* **100** 024315

[85] Ghetta V 2008 *Materials Issues for Generation IV Systems: Status, Open Questions and Challenges* (Dordrecht: Springer Netherlands) p. 513

[86] Kuznetsov R A, Butkalyuk P S, Tarasov V A, Baranov A Yu, Butkalyuk I L, Romanov E G, Kupriyanov V N and Kazakova E V 2012 *Radiochemistry* **54** 383

[87] Hogle S, Boll R A, Murphy K, Denton D, Owens A, Haverlock T J, Garland M and Mirzadeh S 2016 *Appl. Radiat. Isot.* **114** 19

[88] Ma X, Wen W Q, Huang Z K, Wang H B, Yuan Y J, Wang M, Sun Z Y, Mao L J, Yang J C, Xu H S, Xiao G Q and Zhan W L 2015 *Phys. Scr.* **T166** 014012

[89] Barci V, Ardisson G, Barci-Funel G, Weiss B, El Samad O and Sheline R K 2003 *Phys. Rev. C* **68** 034329

[90] Sakharov S L 2010 *Phys. Atom. Nuclei* **73** 1

[91] Von Der Wense L, Seiferle B, Laatiaoui M and Thirolf P G 2015 *Eur. Phys. J. A* **51** 29

[92] Von Der Wense L, Seiferle B, Laatiaoui M, Neumayr J B, Maier H J, Wirth H F, Mokry C, Runke J, Eberhardt K, Düllmann C E, Trautmann N G and Thirolf P G 2016 *Nature* **533** 47

[93] Von Der Wense L, Seiferle B, Laatiaoui M and Thirolf P G 2016 *Nucl. Inst. Methods Phys. Res. B* **376** 260

[94] Seiferle B, Von Der Wense L and Thirolf P G 2017 *Phys. Rev. Lett.* **118** 042501

[95] Scharl K, Ding S, Holthoff G, Hussain M I, Kraemer S, Löbell L, Moritz D, Rozibakieva T, Seiferle B, Zacherl F and Thirolf P G 2023 *Atoms* **11** 108

[96] Moritz D, Scharl K, Wiesinger M, Holthoff G, Teschler T, Hussain M I, López-Urrutia J R C, Dickel T, Ding S, Düllmann C E, Hudson E R, Kraemer S, Löbell L, Mokry C, Runke J, Seiferle B, Von Der Wense L, Zacherl F and Thirolf P G 2025 *Eur. Phys. J. D* **79** 127

[97] Zitzer G, Tiedau J, Okhapkin M V, Zhang K, Mokry C, Runke J, Düllmann Ch E and Peik E 2024 *Phys. Rev. A* **109** 033116

[98] Zitzer G, Tiedau J, Düllmann Ch E, Okhapkin M V and Peik E 2025 *Phys. Rev. A* **111** L050802

[99] Li L, Li Z, Hua X and Tong X 2024 *J. Phys. D: Appl. Phys.* **57** 315205

[100] Steele A V 2008 *Barium Ion Cavity QED and Triply Ionized Thorium Ion Trapping* (Ph. D. Dissertation) (Atlanta: Georgia Institute of Technology)

[101] Wang C, Gan W T, Bai W L, Peng W C and Tong X 2026 *J. Phys. D: Appl. Phys.* **59** 025205

[102] Churchill L R 2010 *Trapping Triply Ionized Thorium Isotopes* (Ph. D. Dissertation) (Atlanta: Georgia Institute of Technology)

[103] Campbell C J 2011 *Trapping, Laser Cooling, and Spectroscopy of Thorium IV* (Ph. D. Dissertation) (Atlanta: Georgia Institute of Technology)

[104] Telnov E Y, Borisyuk P V, Bukharskii N D, Korneev Ph A, Trichev K K and Cherepanov P A 2023 *Rev. Sci. Instrum.* **94** 083302

[105] Kellerbauer A, Kim T, Moore R B and Varfalvy P 2001 *Nucl. Instrum. Methods Phys. Res. A* **469** 276

[106] Itano W M, Bergquist J C, Bollinger J J and Wineland D J 1995 *Phys. Scr.* **T59** 106

[107] Li M, Zhang Y, Zhang Q Y, Bai W L, He S G, Peng W C and Tong X 2022 *J. Phys. B: At. Mol. Opt. Phys.* **55** 035002

[108] Zhang Y, Zhang Q Y, Bai W L, Peng W C, He S G and Tong X 2023 *Chin. J. Phys.* **84** 164

[109] Schwegler N, Holzapfel D, Stadler M, Mitjans A, Sergachev I, Home J P and Kienzler D 2023 *Phys. Rev. Lett.* **131** 133003

[110] Yang Y N, Liu H, He Y H, Yang Z H, Wang M, Chen Y H, She L and Li J M 2014 *Chin. Phys. B* **23** 093702
[111] Feldker T, Fürst H, Hirzler H, Ewald N V, Mazzanti M, Wiater D, Tomza M and Gerritsma R 2020 *Nat. Phys.* **16** 413
[112] Trimby E, Hirzler H, Fürst H, Safavi-Naini A, Gerritsma R and Lous R S 2022 *New J. Phys.* **24** 035004
[113] Xu Z S, Wang H M, Ba Z L and Liu H P 2022 *Chin. Phys. B* **31** 073201
[114] Delahaye P 2019 *Eur. Phys. J. A* **55** 83
[115] Ketterle W 2002 *Rev. Mod. Phys.* **74** 1131
[116] Huang L, Meng Z, Wang P, Peng P, Zhang S L, Chen L, Li D, Zhou Q and Zhang J 2016 *Nat. Phys.* **12** 540
[117] Langen T, Valtolina G, Wang D and Ye J 2024 *Nat. Phys.* **20** 702
[118] Andreev V, Ang D G, DeMille D, Doyle J M, Gabrielse G, Haefner J, Hutzler N R, Lasner Z, Meisenhelder C, O'Leary B R, Panda C D, West A D, West E P and Wu X 2018 *Nature* **562** 355
[119] Lü D S, Ren W, Sun Y, Li T, Qu Q Z, Wang B, Li L, Zhao J B, Zhao X, Ji J W, Ye M F, Xiang J F, Chen W B, Wang Y Z and Liu L 2023 *Natl. Sci. Rev.* **10** nwac180
[120] Li M, Zhang Y, Zhang Q Y, Bai W L, He S G, Peng W C and Tong X 2023 *Chin. Phys. B* **32** 036402
[121] Li Z, Gan W T, Wang C, Hua X and Tong X 2025 *J. Appl. Phys.* **138** 224901
[122] Von Der Wense L, Bilous P V, Seiferle B, Stellmer S, Weitenberg J, Thirolf P G, Pálffy A and Kazakov G 2020 *Eur. Phys. J. A* **56** 176
[123] Von Der Wense L and Zhang C 2020 *Eur. Phys. J. D* **74** 146
[124] Li L, Li Z, Wang C, Gan W T, Hua X and Tong X 2023 *Nucl. Sci. Tech.* **34** 24
[125] Hiraki T, Masuda T, Takatori S, *et al.* 2025 arXiv:2509.00041 [nucl-ex]
[126] Thielking J, Zhang K, Tiedau J, Zander J, Zitzer G, Okhapkin M V and Peik E 2023 *New J. Phys.* **25** 083026
[127] Jeet J 2018 *Search for the low lying transition in the* ^{229}*Th nucleus* (Ph. D. Dissertation) (Los Angeles: University of California)
[128] Lal V, Okhapkin M V, Tiedau J, Irwin N, Petrov V and Peik E 2025 *Optica* **12** 1971
[129] Xiao Q, Penyazkov G, Li X, Huang B, Bu W, Shi J, Shi H, Liao T, Yan G, Tian H, Li Y, Li J, Lu B, You L, Lin Y, Mo Y and Ding S 2025 arXiv:2507.19449 [physics.atom-ph]
[130] Dubin D H E and O'Neil T M 1999 *Rev. Mod. Phys.* **71** 87
[131] Kjærgaard N and Drewsen M 2003 *Phys. Rev. Lett.* **91** 095002
[132] Zhang C, Li P, Jiang J, Von Der Wense L, Doyle J F, Fermann M E and Ye J 2022 *Opt. Lett.* **47** 5591
[133] Porsev S G and Flambaum V V 2010 *Phys. Rev. A* **81** 032504
[134] Müller R A, Volotka A V, Fritzsche S and Surzhykov A 2017 *Nucl. Instrum. Methods Phys. Res. B* **408** 84
[135] Bilous P V, Peik E and Pálffy A 2018 *New J. Phys.* **20** 013016
[136] Wang W, Zou F, Fritzsche S and Li Y 2024 *Phys. Rev. Lett.* **133** 223001
[137] Strizhov V F and Tkalya E V 1991 *Sov. Phys. JETP* **72** 387
[138] Harston M R and Chemin J F 1999 *Phys. Rev. C* **59** 2462
[139] Pálffy A, Evers J and Keitel C H 2007 *Phys. Rev. Lett.* **99** 172502
[140] Wang W, Zhou J, Liu B and Wang X 2021 *Phys. Rev. Lett.* **127** 052501
[141] Wang X 2022 *Phys. Rev. C* **106** 024606
[142] Schaden F, Riebner T, Morawetz I, De Col L T, Kazakov G A, Beeks K, Sikorsky T, Schumm T, Zhang K, Lal V, Zitzer G, Tiedau J, Okhapkin M V and Peik E 2025 *Phys. Rev. Res.* **7** L022036
[143] Terhune J E S, Elwell R, Tan H B T, Perera U C, Morgan H W T, Alexandrova A N, Derevianko A and Hudson E R 2025 *Phys. Rev. Res.* **7** L022062
[144] Morgan H W T, Tran Tan H B, Elwell R, Alexandrova A N, Hudson E R and Derevianko A 2025 *Phys. Rev. Lett.* **134** 253801
[145] Tong X, Hua L, Hua X and Liu X 2025 *Natl. Sci. Rev.* **12** nwaf083
[146] Wang J, Miao H, Ding S and Liu D E 2025 arXiv:2508.10626 [quant-ph]